ORIGINAL PAPER

A forecasting model for the porosity variation during the carbonation process

Gabriella Bretti[1] [ORCID] **· Maurizio Ceseri[1] · Roberto Natalini[1] ·
Maria Carla Ciacchella[2] · Maria Laura Santarelli[2] · Giulia Tiracorrendo[2]**

Abstract

In this paper we introduce a mathematical model of concrete carbonation Portland cement specimens. The main novelty of this work is to describe the intermediate chemical reactions, occurring in the carbonation process of concrete, involving the interplay of carbon dioxide with the water present into the pores. Indeed, the model here proposed, besides describing transport and diffusion processes inside the porous medium, takes into account both fast and slow phenomena as intermediate reactions of the carbonation process. As a model validation, by using the mathematical based simulation algorithm we are able to describe the effects of the interaction between concrete and CO_2 on the porosity of material as shown by the numerical results in substantial accordance with experimental results of accelerated carbonation taken from literature. We also considered a further reaction: the dissolution of calcium carbonate under an acid environment. As a result, a trend inversion in the evolution of porosity can be observed for long exposure times. Such an increase in porosity results in the accessibility of solutions and pollutants within the concrete leading to an higher permeability and diffusivity thus significantly affecting its durability.

1 Introduction

Concrete is by far the most widely used construction material worldwide (Meyer 2005) probably for the concept of eternity that has always been associated with it.

✉ Gabriella Bretti
  g.bretti@iac.cnr.it

[1] Istituto per le Applicazioni del Calcolo "M.Picone", Rome, Italy

[2] Dipartimento di Inmgegneria Chimica Materiali e Ambiente (DICMA), Centro Ric. Sci. Tecn. Cons. Patr. Sto.-Archit. (CISTeC), Univ. di Roma, Sapienza, Rome, Italy

◊ Springer

Instead, when exposed to its intended service environment, concrete is vulnerable to weathering action, chemical attack, abrasion and other process of deterioration influencing its original form, quality and serviceability.

Alkali-aggregate reaction, sulfate attack, steel corrosion and freeze-thaw cycles are among the major processes harming concrete strength. In fact, concrete has a porous structure and its durability is mainly determined by the ability to resist the penetration of aggressive substances. In particular, the carbon dioxide in atmosphere is responsible for one of the most important degradation phenomena: concrete carbonation. The environmental changes of recent decades are leading to a progressive increase of the carbon dioxide concentration in atmosphere. It results in a more and more aggressive environment for both human and building structures.

Concrete carbonation is determined by a series of chemical reactions that consume calcium hydroxide ($Ca(OH)_2$) and form calcium carbonate ($CaCO_3$). The reaction is fueled by carbon dioxide (CO_2), transported by water through the porous medium. It is well known that carbonation weakens buildings and causes serious damages to reinforced concrete. In fact, steel bars contained in the structures are protected from corrosion by a thin film of oxide. Such a layer is formed by the basic environment of the concrete, which has a pH-value of at least 13. In a carbonated zone, however, the overall environment becomes acid with the pH-value falling down to 9. The acid surrounding destroys the protective layer and corrosion of steel bars begins (Pedeferri 2010).

Carbonation has attracted research interests for several reasons. First of all, the structural issues already mentioned: many buildings, or bridges are made of reinforced concrete and knowledge about carbonation can help mitigating damages. Another factor is the complexity of the process that is still not completely understood: this requires a multidisciplinary approach at the intersection of chemistry, engineering, and mathematics. Finally, several historical buildings are made of concrete: mitigation of carbonation can help safeguards Cultural Heritage sites. Some examples of literature addressing with different mathematical models the mechanism of carbonation are (Ahsraf 2016; Chapwanya et al. 2009; Chen et al. 2019; Freddi and Mingazzi 2021; Kashef-Haghighi et al. 2015; Peter et al. 2008; Torgal et al. 2012; Radu et al. 2013; Mitchell et al. 2010). In the recent paper published by some of the authors, i.e. Bretti et al. (2022), a mathematical model formulated as a moving boundary problem was introduced. In particular, some free boundary problems describing the evolution of calcium carbonate stones under the attack of CO_2 dispersed in the atmosphere were introduced, taking into account both the shrinkage of concrete and the influence of humidity on the carbonation process.

The present work, instead, is not focused on the shrinkage phenomenon affecting concrete, but on the description of the porosity variation occurring during the carbonation process as the result of several intermediate chemical reactions involving the interplay of carbon dioxide with the water present into the pores.

The whole carbonation process is caused by diffusion/transport mechanism (that regulate the movement of carbon dioxide and water inside the porous material) and it can be stated by the following chemical equation

$$Ca(OH)_{2(s)} + CO_{2(g)} \longrightarrow CaCO_{3(s)} + H_2O_{(l)}$$
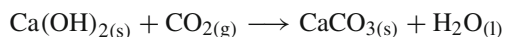
i.e. the gaseous carbon dioxide present in the atmosphere reacts with calcium hydroxide of concrete forming calcium carbonate and water.

The reaction starts from the external surface of the concrete element in the presence of a film of water to gradually penetrate the structure through the pore network characterizing the material. This reaction is the result of a series of equilibria that are established inside the pores of the cement matrix, where an aqueous solution is present (Coppola 2007).

However, such a reaction is the result of a series of intermediate reactions. We can subdivide such reactions in the following successive steps:

(1) Gaseous CO_2 dissolves in the aqueous pores generating carbonic acid ($H_2CO_{3(aq)}$);
(2) Carbonic acid realizes two successive dissociations ending with carbonate (CO_3^{2-}) and two hydrogen ions ($2H^+$); indeed, in general a Portland Cement I (object of the model) has a pH = 12.5−13.8 depending on the composition (Plusquellec et al. 2017), so we are in the conditions of pH>10;
(3) Calcium hydroxide is dissociated in the aqueous solution. Dissociation results in two products:

  (a) Calcium ion (Ca^{2+}), that bonds with carbonate to form calcium carbonate,
  (b) Hydroxide ($2OH^{2-}$), that with the two ions of hydrogen forms two molecules of water.

The above processes describe the carbonation reactions. However, the newly formed calcium carbonate might not be stable. Thus, a new step shall be added:

(4) $CaCO_3$ disassociate itself into a calcium ion and into carbonate.

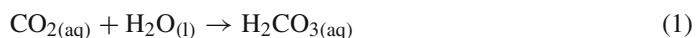To our knowledge, this last step has never been considered by researchers that in general focuses on the formation of $CaCO_3$ only.
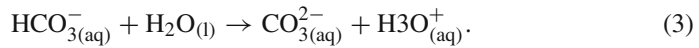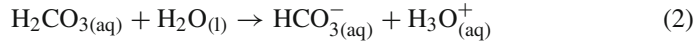
Calcium carbonate is not very soluble in pure water. Although it is possible to estimate a solubility value of about 16 mg/l, it has to be considered that in presence of acidified water, it tends to dissolve and dissociate. In fact, at the normal partial atmospheric pressure of CO_2, the solubility of $CaCO_3$ is quite high, since is about three times higher than its solubility in pure water, see Ogino et al. (1987). When the partial pressure of environmental CO_2 increases, as occurs for example in highly urbanized, industrial environments and in the vicinity of poorly ventilated surfaces, the pH of the solution drops and its solubility increases, for this reason this equilibrium must be considered in the global process (Coto et al. 2012; Mara 2019).

Therefore, this phenomenon might have an important effect on the deterioration of both common and hystorical buildings. A careful evaluation of this step by combining it with the carbonation process is particularly needed.

Thus, as can be seen, the general carbonation reaction of concrete is the result of a series of intermediate equilibria. In the model that will be described, the global process is considered through three main reactions.

1.1 Carbonic acid formation and rapid dissociation

$$CO_{2(aq)} + H_2O_{(l)} \rightarrow H_2CO_{3(aq)} \tag{1}$$

$$H_2CO_{3(aq)} + H_2O_{(l)} \rightarrow HCO_{3(aq)}^- + H_3O_{(aq)}^+ \tag{2}$$

$$HCO_{3(aq)}^- + H_2O_{(l)} \rightarrow CO_{3(aq)}^{2-} + H3O_{(aq)}^+. \tag{3}$$

The two dissociation reactions of carbonic acid are extremely fast, while the hydration reaction of CO_2 is slow, so it is this latter reaction that controls step 1 of the process. As a result the CO_3^{2-} ion can be directly considered as the final product of the three equilibria and the slow kinetics of carbonic acid formation.

1.2 Formation of calcium carbonate

Strictly, it should consider first the dissociation reaction of calcium hydroxide and then the subsequent equilibria that lead to the formation of $CaCO_3$:

$$Ca(OH)_{2(s)} \rightarrow Ca_{(aq)}^{2+} + 2OH]_{(aq)}^-. \tag{4}$$
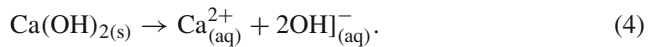
Nevertheless, considering that the previous reaction is nearly instantaneous and taking into account that the diffusion coefficient of calcium hydroxide is very low, the concentration of the calcium ions in solution can be directly considered. From the reaction stoichiometry $[Ca(OH)_2] = [Ca^{2+}]$, we can write the reaction that leads to the formation of calcium carbonate in the following way:

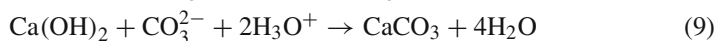$$Ca(OH)_{2(s)} + CO_{3(aq)}^{2-} + 2H_3O_{(aq)}^+ \rightarrow CaCO_{3(s)} + 4H_2O_{(l)}. \tag{5}$$
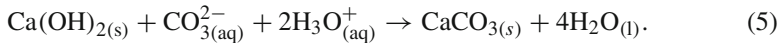
The initial conditions—that will be defined later—will consider the concentration of the calcium ion in solution.

1.3 Dissolution of the calcium carbonate in the aqueous phase

With the aim of a better understanding of the microstructural changes in the material due to carbonation, after the formation of calcium carbonate, the following dissociation equilibrium is finally considered:

$$CaCO_{3(s)} + H_3O_{(aq)}^+ \rightleftarrows Ca_{(aq)}^{2+} + HCO_{3(aq)}^- + H_2O_{(l)}. \tag{6}$$

Summing up, in our study, we are going to consider the following chemical reactions:

$$CO_2 + H_2O \rightarrow H_2CO_3 \tag{7}$$

$$H_2CO_3 \rightarrow HCO_3^- + H_3O^+ \rightarrow CO_3^{2-} + 2H_3O^+ \tag{8}$$

$$Ca(OH)_2 + CO_3^{2-} + 2H_3O^+ \rightarrow CaCO_3 + 4H_2O \tag{9}$$

$$CaCO_3 + H_3O^+ \rightarrow Ca^{2+} + HCO_3^- + H_2O. \tag{10}$$

Due to the multiplicity of phenomena—i.e. transport, diffusion and chemical reactions and the great variability of concrete in terms of composition and microstructure,

the construction of reliable forecast models is complex. In addition, the carbonation process is known to depend on several parameters. Among the different parameters, we can mention: the water/cement ratio, the carbon dioxide concentration in the environment, the ambient moisture. While the first is a structural property of concrete, the other two depends on the environmental conditions and in general cannot be controlled (Pedeferri 2010).

The carbonation mechanism is a rather slow process in ambient conditions. In order to speed up experimental settings, several authors set cement specimen in accelerated conditions, i.e., they increase the concentration of carbon dioxide in a laboratory room above the natural exposure values. A higher concentration of carbon dioxide in the atmosphere increases the internal-external concentration gradient, consequently increasing the diffusion speed towards the cement matrix and therefore the possibility of reacting with the concrete (Pu et al. 2012). To give some numbers, in a natural environment, carbon dioxide concentration varies in the range [0.03–1%]. It has been shown that for 20% carbon dioxide concentration, the carbonation front can reach in one week the same depth reached by the natural carbonation front in one year. In general, numerous studies agree that for CO_2 concentrations as high as 3.5%, accelerated carbonation is comparable to natural carbonation (Auroy et al. 2018). Accelerated carbonation was not always found to be representative of natural carbonation, especially for the microstructural changes of the material. It is recommended that a 20% CO_2 limit is not exceeded to allow comparison with natural carbonation (Anstice et al. 2005; Groves et al. 1990; Leemann and Moro 2017).

Another manageable parameter to accelerate carbonation is humidity. Reliable results can be obtained exposing samples to relative humidity (RH) ranging from 50 to 70%, values for which the carbonation rate was found to be maximal. It represents a compromise between the disadvantaged transport of CO_2 in the aqueous phase and the reaction that occurs only in the presence of water (Galan et al. 2013). Temperature favors the diffusion of CO_2 towards the concrete, up to 60 ° C the absorption of carbon dioxide increases with the temperature (Pu et al. 2012; Sun 2011).

Carbonation generates important changes in concrete microstructure, a consequence of the chain reactions that takes place. As mentioned, the most important and representative parameter of these changes is the study of the porosity of the material. The dissolution of calcium hydroxide occurs almost instantaneously, the porosity that is formed as a result of this reaction is immediately occupied by the precipitation of calcium carbonate, a compound characterized by an approximately 11.7% greater volume. Following the formation of $CaCO_3$, the porosity of the material is reduced (Ishida and Li 2008).

Considering the effect of carbon dioxide on the solubility of the formed $CaCO_3$, the calcium carbonate in turn tends to dissociate in water (Coto et al. 2012), the porosity will consequently increase over time. Therefore, stop modeling at the decrease in porosity generated by the formation of $CaCO_3$ is misleading for final data interpretation. According to the authors it is mandatory to consider the reaction (4) and to monitor the system evolution over time. Only in this way it will be possible to have an in-depth description of the degradation phenomenon of the material. The goal of this work is to provide a more accurate mathematical forecasting model that considers simultaneously the transport and diffusion phenomena, the totality of the chemical

reactions of the process, and the evolution over time of cement that has undergone carbonation. The dissolution reaction of the $CaCO_3$ formed is here considered and it results in a change in porosity not foreseen by classic models.

2 Materials and methods

Literature provides many experiments for the evaluation of the effects of carbonation on cement materials. As mentioned, the phenomenon in natural conditions is very slow, that is the reason why most of the experiments are carried out in conditions of accelerated carbonation. Typically 2–10 cm in size concrete samples are selected. After casting, test specimens are cured for 28 days, in order to allow the concrete to reach the appropriate resistance. Two ends of each cylinder are coated with epoxy resin or paraffin wax to ensure that carbon dioxide could diffuse only into the specimens in a two-dimensional mode. Once selected the test conditions (i.e. CO_2 concentration, temperature, humidity and time), the samples are transferred to a sealed chamber and subjected to carbonation (Chang and Chen 2006).

At the end of the test, the specimens are splitted, the freshly split surface is cleaned and sprayed with a phenolphthalein pH indicator. This indicator turns color depending of pH concrete. In the non-carbonated part, where the concrete is still highly alkaline, a purple-red colour is obtained. In the carbonated part of the specimen where the pH is reduced, no coloration occurred (Villain and Thiery 2006). From this simple test, the carbonation depth can be derived, as shown in Fig. 1, where a picture of a laboratory test on a concrete sample reacting to the phenolphthalein is represented.

Other more in-depth analysis can be performed to quantify the effect of carbonation on the material. SEM microscope observations and X-rays analyses are generally preferred to identify the presence of $CaCO_3$ formed and residual $Ca(OH)_2$ not yet reacted with CO_2. From the comparison of the sample before and after carbonation, it is easy to see the transition from a structure rich in calcium hydroxide and a structure mainly composed of $CaCO_3$, which clearly indicates the reaction with CO_2 has taken place (Thiery et al. 2007; Villain et al. 2007).

To evaluate the effect of carbonation on porosity, fundamental parameter for process control, gammadensimetry and mercury intrusion analysis can be chosen. To test

Fig. 1 Carbonation depth obtained from the phenolphthalein spray test (mm). As can be observed, the sample is coloured pink only in the portion not yet carbonated (right side)
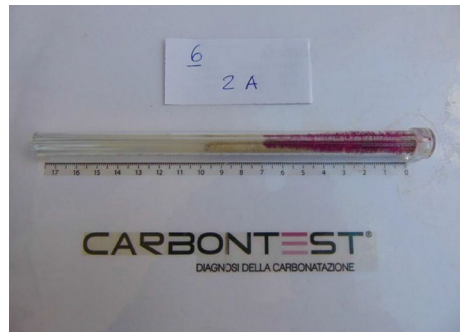
Table 1 Material characteristics of the specimen considered in our study. Values taken from Pan et al. (2018)	Design strength	w/c	Water: kg/m^3	Cement: kg/m^3
	CP30	0.53	622	1179

the mathematical model we referred to a carbonation experiment (Pan et al. 2018) performed on a type Portland cement specimen, with the characteristics detailed in Table 1:

As mentioned, the specimens are first polymerized, in this case at 20 °C and 70% relative humidity for 24 h and then turned out and placed in a seasoning environment at 20 ± 3 °C and 90% RH for 28 days. Subsequently, samples are placed in a drying oven at 50 °C for 48 h. The carbonation test is carried out at T = 20 °C and 70% humidity for CO_2 concentrations 0.03, 3 and 20%.

3 The mathematical model

The process of carbonation takes place into water that penetrates the porous matrix transporting the aggressive substances (i.e. carbon dioxide and carbonic acid). Thus, we have to consider the filtration of water and the transport and diffusion phenomena of such substances. Moreover, we have to take into account the chemical reactions involved.

Water movement

First of all we consider the movement of water into the porous matrix, i.e.

$$\frac{\partial w}{\partial t} = -\frac{\partial}{\partial z} F(w) + r_w,$$

where w is the moisture content and r_w a chemical reaction term that will be specified later on.

F is the water flux into the concrete and is given by the Darcy's law

$$F(w) = -D(w, \varepsilon) \frac{\partial w}{\partial z},$$

with $D(w, \varepsilon)$ is water diffusivity and depends on both the moisture content and porosity (in general, we have that $0 \leq w \leq \varepsilon$). A possible choice for diffusivity is Chapwanya et al. (2009):

$$D(w, \varepsilon) = \left(\frac{\varepsilon - w_{min}}{\varepsilon_0 - w_{min}} \right)^{\frac{19}{6}} D^*(w)$$

with w_{min} is the residual water content, ε_0 is the initial porosity and $D^*(w)$ the following function:

$$D^*(w) = Ae^{Bw}$$

with A and B shape parameters for water diffusivity, suitable constants taken from Chapwanya et al. (2009) and reported in Table 2.

Carbon dioxide

We describe the aqueous phase of carbon dioxide. In this setting, and after being dissolved in water, CO_2 is subject to three processes: water transport through the porous matrix; aqueous diffusion according to Fick's law; chemical reactions. All of the above processes are included in the following equation

$$\frac{\partial(wa)}{\partial t} = \underbrace{\frac{\partial}{\partial z}\left(D(w,\varepsilon)a\frac{\partial w}{\partial z}\right)}_{\text{transport}} + \underbrace{\frac{\partial}{\partial z}\left(D_a w\frac{\partial a}{\partial z}\right)}_{\text{diffusion}} + \underbrace{r_a}_{\text{reaction}}$$

where a is the concentration of carbon dioxide and D_a is its diffusivity in water.

Carbonate

We then proceed to describe carbonate evolution in water. To be precise, we should have described the evolution of carbonic acid. However, since carbonic acid dissolves very quickly, we can model directly the transport, diffusion, and chemical processes involving carbonate. As it is the case of carbon dioxide, carbonate is subject of transport and diffusion in water. Moreover, it is involved in two chemical reactions: the first one between water and carbon dioxide forming carbonate; the second one between carbonate and calcium hydroxide. All the above processes are summed up into the following equation

$$\frac{\partial(wb)}{\partial t} = \frac{\partial}{\partial z}\left(D(w,\varepsilon)b\frac{\partial w}{\partial z}\right) + \frac{\partial}{\partial z}\left(D_b w\frac{\partial b}{\partial z}\right) + r_b.$$

Calcium hydroxide

Calcium hydroxide consumes when in contact with carbonate. In what follows, we assume that calcium hydroxide is subjected only to this chemical reaction and is not transported nor it diffuses in water. Thus, it evolves according to the following equation:

$$\frac{\partial i}{\partial t} = r_i.$$

Calcium carbonate

Calcium carbonate is the result of two reactions: it is produced by the reaction between calcium hydroxide and carbonate; it dissolves by the production of carbonate and calcium ions.

$$\frac{\partial c}{\partial t} = r_c.$$

Calcium ion

Finally, calcium ion is produced by the dissolution of calcium carbonate

$$\frac{\partial e}{\partial t} = r_e.$$

3.1 Chemical reaction terms

Using the procedure outlined in Alì et al. (2007), we define the reaction terms as follows

$$r_w = m_w(\omega_{ib} - \omega_a), \tag{11}$$

$$r_a = -m_a\omega_a, \tag{12}$$

$$r_b = -m_b(\omega_{ib} - \omega_a), \tag{13}$$

$$r_i = -m_i\omega_{ib}, \tag{14}$$

$$r_c = m_c(\omega_{ib} - \omega_c), \tag{15}$$

$$r_e = m_e\omega_c, \tag{16}$$

where the terms $m_k, \ k = w, a, b, i, c, e$ indicates the molar masses of the respective substances, while the ω's describe the single chemical reactions and are defined as follows:

$$\omega_a = v\frac{a}{m_a},$$

$$\omega_{ib} = \mu\left(\frac{i}{m_i} \cdot \frac{b}{m_b}\right),$$

$$\omega_c = \delta\frac{c}{m_c},$$

with v, μ e δ the reaction rates.

3.2 Porosity

One of the main consequences of carbonation is the change of porosity (ε). In particular, porosity will change due to the following processes:

(1) Calcium hydroxide dissolution with the resulting formation of calcium carbonate,
(2) Dissolution of calcium carbonate.

The first process will lower the value of the porosity, while the second will increase it. Thus, porosity will depends on the concentration of calcium hydroxide, calcium carbonate, and calcium ion, i.e. $\varepsilon = \varepsilon(i, c, e)$. However, we can represent porosity as function of only calcium hydroxide and calcium ion. In fact, we have that:

$$\frac{\partial}{\partial t}\left(\frac{i}{m_i} + \frac{c}{m_c} + \frac{e}{m_e}\right) = 0,$$

i.e.

$$\frac{i}{m_i} + \frac{c}{m_c} + \frac{e}{m_e} = \frac{i_0}{m_i} + \frac{c_0}{m_c} + \frac{e_0}{m_e},$$

where i_0, c_0 and e_0 are the initial concentrations of calcium hydroxide, calcium carbonate, and calcium ion, respectively. Then, we can express function c in terms of i and e. Following the same arguments of Alì et al. (2007), we define the porosity as

$$\varepsilon = \varepsilon_1 + (\varepsilon_0 - \varepsilon_1)\frac{i}{i_0} + \varepsilon_2\left(\frac{e}{e_0} - 1\right), \tag{17}$$

where:

ε_0 is the initial porosity,
ε_1 is the porosity when calcium hydroxide is completely consumed,
ε_2 is the variation of porosity due to dissociation of calcium carbonate.

The values of the above parameters that we chose for our simulations are listed in Table (2); here we report some comments on how we chose those values.

In general, the porosity of concrete is a datum; in our case we took a value $\varepsilon_0 = 0.2$ as reported in Papadakis et al. (1989).

The value of ε_1 has been chosen from reference (Pan et al. 2018, Table 7), where values of carbonated stones are listed for several carbon dioxide concentrations; in particular, we choose the value between the resulting porosities of stones exposed at 3% and 20% CO_2 concentrations.

Regarding ε_2, its choice is much more involved. In fact, we could not find any reference in the literature permitting us to estimate a credible value for such parameter, thus we apply two different approaches to find it. Since we followed the methods in Alì et al. (2007), we first use the theoretical approach given by the following expression:

$$\varepsilon_2 = \frac{V_c}{m_e}e_0,$$

with V_c the molar volume of calcium carbonate, while the other constants have been already defined above. Thus, we can determine the value of ε_2 as $8.2 \cdot 10^{-3}$.

On the other hand, we can also proceed as follows. After a lot of time, we can imagine that both carbon hydroxide and calcium carbonate will be completely consumed by

the described chemical reactions. Thus, as t goes to infinity, we have the following expression for calcium ion:

$$e_\infty = e_0 + m_e \left(\frac{i_0}{m_i} + \frac{c_0}{m_c} \right),$$

while for porosity we obtain:

$$\varepsilon = \varepsilon_1 + \varepsilon_2 \left(\frac{e_\infty}{e_0} - 1 \right) = \varepsilon_1 + \varepsilon_2 \frac{m_e}{e_0} \left(\frac{i_0}{m_i} + \frac{c_0}{m_c} \right).$$

If we also assume that for long time the porosity will increase to its maximum value, i.e. $\varepsilon = 1$, by using the values in Table 2 we can estimate ε_2 as:

$$\varepsilon_2 = \frac{1 - \varepsilon_1}{\frac{i_0}{m_i} + \frac{c_0}{m_c}} \frac{e_0}{m_e} = 0.29.$$

In the end, we determined a range of values for ε_2, that is

$$\varepsilon_2 \in [8.2 \cdot 10^{-3}, 2.9 \cdot 10^{-1}].$$

However, the upper bound on such an estimate is quite large, since it is difficult that porosity will attain its maximum value.

The complete model

Summing up, the complete model reads as:

$$\frac{\partial w}{\partial t} = \frac{\partial}{\partial z} \left(\left(\frac{\varepsilon - w_{min}}{\varepsilon_0 - w_{min}} \right)^{\frac{19}{6}} D^*(w) \frac{\partial w}{\partial z} \right) + r_w \tag{18}$$

$$\frac{\partial (wa)}{\partial t} = \frac{\partial}{\partial z} \left(a \left(\frac{\varepsilon - w_{min}}{\varepsilon_0 - w_{min}} \right)^{\frac{19}{6}} D^*(w) \frac{\partial w}{\partial z} \right) + \frac{\partial}{\partial z} \left(D_a w \frac{\partial a}{\partial z} \right) + r_a \tag{19}$$

$$\frac{\partial (wb)}{\partial t} = \frac{\partial}{\partial z} \left(b \left(\frac{\varepsilon - w_{min}}{\varepsilon_0 - w_{min}} \right)^{\frac{19}{6}} D^*(w) \frac{\partial w}{\partial z} \right) + \frac{\partial}{\partial z} \left(D_b w \frac{\partial b}{\partial z} \right) + r_b \tag{20}$$

$$\frac{\partial i}{\partial t} = r_i \tag{21}$$

$$\frac{\partial e}{\partial t} = r_e \tag{22}$$

$$\frac{c}{m_c} = \frac{i_0}{m_i} + \frac{c_0}{m_c} + \frac{e_0}{m_e} - \frac{i}{m_i} - \frac{e}{m_e} \tag{23}$$

$$\varepsilon = \varepsilon_1 + (\varepsilon_0 - \varepsilon_1) \frac{i}{i_0} + \varepsilon_2 \left(\frac{e}{e_0} - 1 \right). \tag{24}$$

3.3 Initial and boundary conditions

To complete the mathematical model, we need to impose suitable initial and boundary conditions for the unknown functions. In what follows we consider a concrete specimen in the domain $[0, L]$, with $L > 0$. The boundary $z = 0$ identifies the surface in contact with the ambient air; the porous medium exchanges humidity, carbon dioxide, and carbonate with the environment through this boundary.

First of all, we do not need to define boundary conditions for the variables i, c, and e, since these are solutions of ODEs. The spatial evolution of calcium hydroxide, calcium carbonate, and calcium ion depends on the spatial evolution of the other variables. Concerning the other unknowns, we impose a zero flux condition at the right boundary $z = L$, i.e.

$$\frac{\partial f}{\partial z} = 0 \ \text{ for } f = w, a, b.$$

Concerning the surface in contact with ambient air, we impose a Dirichlet condition for water, i.e.

$$w(0, t) \equiv \bar{w}$$

where the constant $\bar{w}$ is the value of the environmental moisture content computed as $\bar{w} = SVD(T) * RH$, where SVD is the saturated vapor density in $[g/cm^3]$ computed as in Bretti et al. (2022):

$$SVD(T) = 10^{-6} \times (5.018 + 0.32321T + 8.1847 \times 10^{-3}T^2 + 3.1243 \times 10^{-4}T^3), \quad (25)$$

for a relative humidity of $RH = 80\%$ and temperature $T = 25\,^\circ C$.

Then we impose flux condition at the left boundary for carbon dioxide, i.e.

$$\frac{\partial a}{\partial z}(0, t) = -K_a(a(0, t) - \bar{a}),$$

with K_a an unknown constant describing the penetration rate of carbon dioxide that will be determined by calibration and $\bar{a}$ the value of external carbon dioxide concentration, meaning that the flux of carbon dioxide depends on the difference between internal and external carbon dioxide concentration. Moreover, we assume null-flux condition at the left boundary for carbonate:

$$\frac{\partial b}{\partial z}(0, t) = 0.$$

The mathematical model will describe the evolution of the carbonation process in the time interval $[0, T]$, with $T > 0$. For each of the functions we impose suitable initial conditions of the form

$$f(z, 0) \equiv f_0 \ \text{ for } f = w, a, b, c, i, e.$$

The values of the parameters introduced in this Section are listed in Table 2.

4 Numerical approximation of the mathematical model

We mesh the interval $[0, L]$ with a step $\Delta z = \frac{L}{N+2}$ and we denote

$$\lambda = \frac{\Delta t}{\Delta z}, z_j = j\Delta z, j = 0, ..., N + 1.$$

We also set $w_j^n = w(z_j, t_n)$ the approximation of the function w at the height z_j and at the time t_n. A consistent approximation of $\partial_z(u(z)\partial_z v)$ by means of Taylor expansions is the following first order approximation:

$$\Delta_j(u, v) := \frac{(u_j + u_{j+1})(v_{j+1} - v_j) - (u_{j-1} + u_j)(v_j - v_{j-1})}{2\Delta z^2}.$$

Then, the discretization in explicit form of equation (18) is:

$$\frac{w_j^{n+1} - w_j^n}{\Delta t} = D_w \Delta_j \left(\left(\frac{\varepsilon - w_{min}}{\varepsilon_0 - w_{min}} \right)^{\frac{19}{6}}, w^n \right)$$
$$+ \frac{m_w \mu}{m_i m_b} \frac{i_j^{n+1} b_j^n + i_j^n b_j^{n+1}}{2} - \frac{\nu m_w}{m_a} a_j^n. \tag{26}$$

Note that in the formula above we approximate the reaction term $m_w(\omega_{ib} - \omega_a)$ with the non-standard approximation for source terms already applied in Reale et al. (2019). Now, if we consider the velocity field computed in the Eq. (26) and we set it as $V = D_w \left(\frac{\varepsilon - w_{min}}{\varepsilon_0 - w_{min}} \right)^{\frac{19}{6}} \partial_z w$, we can rewrite Eqs. (19) and (20), respectively, as:

$$\partial_t(wa) - D_w \partial_z(aV) = D_a \partial_z(w\partial_z a) - \nu a, \tag{27}$$

and

$$\partial_t(wb) - D_w \partial_z(bV) = D_b \partial_z(w\partial_z b) - \frac{\mu}{m_i}ib + \nu a\frac{m_b}{m_a} + \delta c\frac{m_b}{m_c}. \tag{28}$$

We can assume:

$$V_j^n = D_w \left(\frac{\varepsilon_j^n - w_{min}}{\varepsilon_0 - w_{min}} \right)^{\frac{19}{6}} \frac{w_{j+1}^n - w_{j-1}^n}{2\Delta z}, \quad \text{for } j = 1, \ldots, N,$$

with the boundary values set as follows:

$$V_0^n = 0;$$
$$V_{N+1}^n = 0.$$

Therefore, the approximation scheme for (27) reads as:

$$\frac{(wa)_j^{n+1} - (wa)_j^n}{\Delta t} = \frac{V_{j+1}^n a_{j+1}^n - V_{j-1}^n a_{j-1}^n}{2\Delta z}$$
$$+ \frac{|V_{j+1}^n| a_{j+1}^n - 2|V_j^n| a_j^n + |V_{j-1}^n| a_{j-1}^n}{2\Delta z}$$
$$+ D_a \Delta_j(w^n, a^n) - va_j^{n+1}.$$

For discretizing (28) we apply an implicit-explicit approximation scheme for the reaction term:

$$\frac{(wb)_j^{n+1} - (wb)_j^n}{\Delta t} = \frac{V_{j+1}^n b_{j+1}^n - V_{j-1}^n b_{j-1}^n}{2\Delta z}$$
$$+ \frac{|V_{j+1}^n| b_{j+1}^n - 2|V_j^n| b_j^n + |V_{j-1}^n| b_{j-1}^n}{2\Delta z}$$
$$+ D_b \Delta_j(w^n, b^n) - \frac{\mu}{2m_i}(i_j^{n+1} b_j^n + i_j^n b_j^{n+1})$$
$$+ \frac{m_b}{m_a} va_j^n.$$

The scheme above is convergent under the CFL condition

$$\Delta t \leq \Delta^2 z / D_a.$$

Then, using an implicit-explicit approximation of equation (21), we can write the discretized problem as:

$$w_j^{n+1} = w_j^n + \Delta t D_w \Delta_j \left(\left(\frac{\varepsilon - w_{min}}{\varepsilon_0 - w_{min}} \right)^{\frac{19}{6}}, w^n \right)$$
$$+ \Delta t m_w \left(\frac{\mu}{m_i m_b} \frac{i_j^{n+1} b_j^n + i_j^n b_j^{n+1}}{2} - \frac{va_j^n}{m_a} \right), \quad j = 1, \ldots, N,$$

$$a_j^{n+1} = \frac{1}{w_j^n + v\Delta t} \left\{ (wa)_j^n + \Delta t \frac{|V_{j+1}^n| a_{j+1}^n - 2|V_j^n| a_j^n + |V_{j-1}^n| a_{j-1}^n}{2\Delta z} \right.$$
$$+ \Delta t \frac{V_{j+1}^n a_{j+1}^n - V_{j-1}^n a_{j-1}^n}{2\Delta z} + \Delta t D_a \Delta_j(w^n, a^n) \left. \right\}, \quad j = 1, \ldots, N,$$

$$b_j^{n+1} = \frac{1}{w_j^n + \Delta t \frac{\mu}{2m_i} i_j^n} \left\{ (wb)_j^n + \Delta t \frac{|V_{j+1}^n| b_{j+1}^n - 2|V_j^n| b_j^n + |V_{j-1}^n| b_{j-1}^n}{2\Delta z} \right.$$
$$+ \Delta t \frac{V_{j+1}^n b_{j+1}^n - V_{j-1}^n b_{j-1}^n}{2\Delta z} + \Delta t D_b \Delta_j(w^n, b^n)$$

$$+ \Delta t \frac{\nu m_b}{m_a} a_j^n - \Delta t \frac{\mu}{2 m_i} i_j^{n+1} b_j^n \Big\}$$

$$j = 1, \ldots, N,$$

$$i_j^{n+1} = \frac{1}{1 + \frac{\Delta t}{2} \frac{\mu b_j^n}{m_b}} \left\{ i_j^n - \frac{\Delta t}{2} \frac{\mu}{m_b} i_j^n b_j^{n+1} \right\},$$

$$e_j^{n+1} = e_j^n + \Delta t \delta \frac{m_e}{m_c} c_j^n,$$

$$c_j^{n+1} = c_0 + m_c \left(\frac{1}{m_i} (i_0 - i_j^n) + \frac{1}{m_e} (e_0 - e_j^n) \right), \tag{29}$$

$$\varepsilon_j^{n+1} = \varepsilon_1 + (\varepsilon_0 - \varepsilon_1) \frac{i_j^n}{i_0} + \varepsilon_2 \left(\frac{e_j^n}{e_0} - 1 \right). \tag{30}$$

with suitable discretization of boundary conditions for w, a and b described above.

5 Numerical results

For the numerical tests we assumed the values of the parameters reported in Table 2.

Considering that the values of the chosen kinetic constants refer to an aqueous solution under ideal conditions, it was decided to act on these parameters. In Fig. 2 the plots of the profiles of the quantities obtained by the algorithm based on the mathematical model (18–24) are depicted assuming all the parameters as in Table 2 at the initial time $t = 0$ (on the left) and at $t = 28$ days (on the right). Notice that time $t = 0$ represents the time when the the diffusion of CO_2 in the aqueous phase has already taken place in the cement matrix and the carbonic acid formation reaction has begun. Indeed, the $CO_{2(g)} \rightarrow CO_{2(aq)}$ reaction that is regulated by Henry's law was not included in the model, but was directly considered the diffusion of carbon dioxide in the aqueous phase. This choice is also justified because the diffusion coefficient in the gas phase is greater than the one in the liquid phase (Chen et al. 2019).

As shown in Fig. 2, the model perfectly describes the real phenomenon: carbon dioxide a (magenta line) penetrates the material and is immediately consumed, the reaction leads to the consumption of water w (blue line) which in fact decreases. The carbonate ion b is the result of two equilibria, the first in which it forms (8) and the second in which it is consumed to form $Ca\,CO_3$ (9); the yellow curve that describes the trend of b represents the sum of these two reactions. Calcium hydroxide i decreases due to the rapid dissolution reaction until it reaches a minimum value and then increases without returning to the initial value (green line); in a similar way the calcium carbonate c, considered zero at the beginning, is formed until it reaches a maximum and then decreases due to the reaction that leads to its dissolution (red line). The calcium ion e, for the considerations made previously relating to the rapid dissolution of calcium hydroxide, is involved only in the dissociation reaction of calcium carbonate, during which it is consumed (black line).

As can be seen from the porosity profile ε, represented with a cyan line at the bottom of the same Figure, the carbonation process leads to an increase in the porosity value.

Table 2 Parameters of the model (18–24)

	Description	Units	Value	Ref
h	Specimen's height	cm	2	Datum
Δz	Space step	cm	0.1	–
Δt	Time step	s	4	–
A	Shape coefficient of water diffusivity	cm²/s	3.24e−8	Chapwanya et al. (2009)
B	Shape coefficient of water diffusivity	–	100	Chapwanya et al. (2009)
ε_0	Porosity of the unperturbed material	–	0.2	Papadakis et al. (1989)
ε_1	Porosity after complete consumption of Ca(OH)$_2$	–	0.08	Pan et al. (2018)
ε_2	Porosity change due to CaCO$_3$ Dissolution	–	0.015	Hypothesis
D_a	Diffusivity of CO$_2$ in water at 25 °C	cm²/s	1.92×10^{-5}	Zeebe (2011)
D_b	Diffusivity of CO$_3^{2-}$ in water at 25 °C	cm²/s	0.81×10^{-5}	Zeebe (2011)
ρ_w	Density of water	g/cm³	1	Ball (2008)
ν	Coefficient of reaction between CO$_2$ and water at 25 °C and 1 atm	s⁻¹	6	Calibrated against data
μ	Coefficient of reaction between Ca(OH)$_2$ and CO$_3^{2-}$ at 25 °C and 1 atm	cm³/(mol s)	7×10^{-2}	Calibrated against data
δ	Dissolution rate of CaCO$_3$ at 25 °C and 1 atm	s⁻¹	6×10^{-7}	Calibrated against data
m_a	Molecular mass of CO$_2$	g/mol	44.01	Shriver et al. (1990)
m_b	Molecular mass of CO$_3^{2-}$	g/mol	60.01	Shriver et al. (1990)
m_c	Molecular mass of CaCO$_3$	g/mol	100.09	Shriver et al. (1990)

Table 2 continued

|	Description	Units	Value	Ref
m_e	Molecular mass of Ca^{2+}	g/mol	40.08	Shriver et al. (1990)
m_i	Molecular mass of $Ca(OH)_2$	g/mol	74.10	Shriver et al. (1990)
m_w	Molecular mass of water	g/mol	18.01	Shriver et al. (1990)
w_0	Initial water content	g/cm^3	0.622	Pan et al. (2018)
a_0	Initial concentration of CO_2	g/cm^3	3×10^{-4}	Hypothesis
b_0	Initial concentration of CO_3^{2-}	g/cm^3	1.3×10^{-11}	Hypothesis
i_0	Initial concentration of $Ca(OH)_2$	g/cm^3	5.2×10^{-2}	Pan et al. (2018)
e_0	Initial concentration of Ca^{2+}	g/cm^3	8.9×10^{-3}	Hypothesis
c_0	Initial concentration of $CaCO_3$	g/cm^3	0	Hypothesis
$\bar{w}$	Moisture content of the ambient air for $UR = 80\%$, $T = 25\,^\circ C$	g/cm^3	1.6×10^{-3}	Eq. 25
$\bar{a}$	Concentration of CO_2 at the boundary	g/cm^3	4×10^{-3}	Datum
K_a	Penetration rate of CO_2 in the medium	cm^{-1}	10^4	Calibrated against data
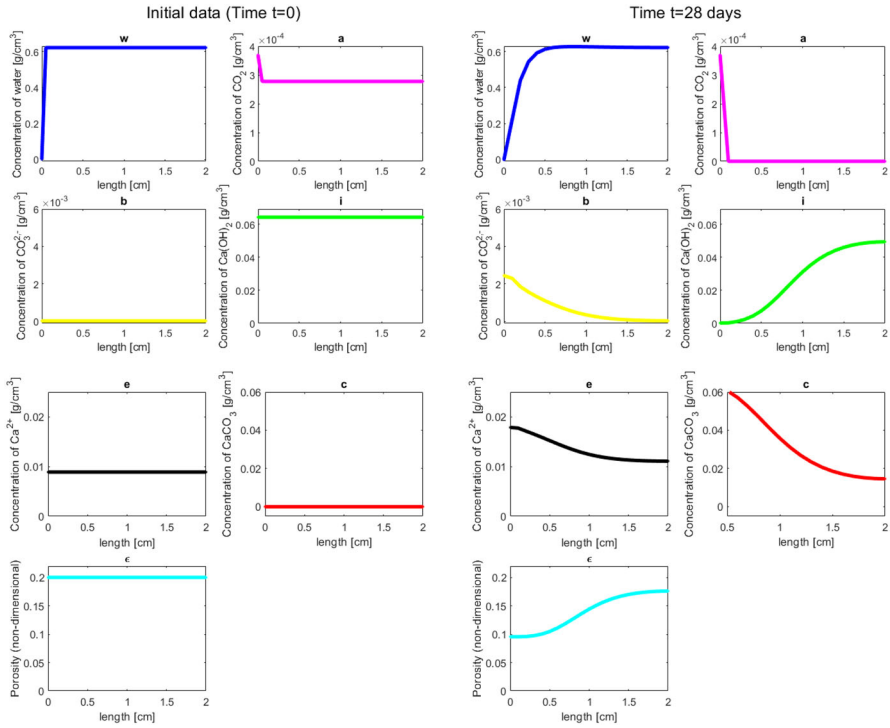
Fig. 2 Profiles of numerical solutions to the system (18–24) at time $t = 0$ (on the left) and $t = 28$ days (on the right), obtained with model parameters in Table 2 and with concentration of carbon dioxide of 20%. The depicted variables are the concentration of water, carbon dioxide, carbonate, calcium hydroxide, calcium carbonate, and calcium ion (in g/cm^3) and the non dimensional porosity profile (cyan line). The figures depict the profile on the space dimension (length of the specimen in *cm*) (color figure online)

However, for longer times, see the right picture in Fig. 3, we observe a decreasing trend up to the spatial coordinate corresponding to the point of penetration of the external agents in the sample and after that point, an increasing profile that reaches the value ε_0 is observed.

Moreover, in the left picture of Fig. 3 we depict the profile of the porosity at the left endpoint x_0 for time $T = 56$ for three different values of ε_2, i.e. $\varepsilon_2 = 0.009, 0.015, 0.025$. As can be observed, the qualitative behavior of the porosity is substantially the same, since the porosity initially decreases and then, after about 20 days starts increasing. Assuming higher/smaller values for ε_2 determines a higher/smaller curvature of the porosity profile.

In conclusion, looking at the graphs depicted above, the main features of our model are on one hand its ability of reproducing the formation as well as the consumption of $CaCO_3$ and, on the other hand, the change in the behavior of porosity.
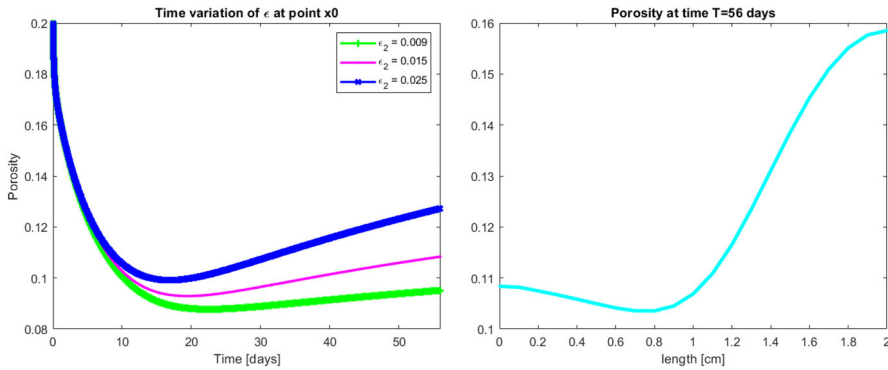
Fig. 3 Left panel: Profile of the porosity at x_0 across $[0, 56]$ days for $\varepsilon_2 = 0.008$ (green curve), $\varepsilon_2 = 0.015$ (magenta curve), $\varepsilon_2 = 0.025$ (blue curve). Right panel: Profile of the porosity at time $T = 56$ days for $\varepsilon_2 = 0.015$ (color figure online)

5.1 Comparison with experimental data

Here we present some numerical tests to make a validation of our model against laboratory outcomes. A multiplicity of data obtained on cementitious materials following accelerated carbonation tests are available in scientific literature, (García-González et al. 2006; Hussain et al. 2016; Kashef-Haghighi et al. 2015; Pan et al. 2018; Talukdar et al. 2012). Accelerated carbonation experiments differ in the imposed starting parameters that usually vary in the following ranges: a CO_2 concentration between 3 and 20%, for a relative humidity in the range 60–70%, with a temperature in the chamber varying between 25 and 35 °C. Observations are generally performed at 7, 14 and 28 days. We refer to data contained in Pan et al. (2018) where the initial parameters set are those most frequently found in literature. More in detail, in Pan et al. (2018) where the content of calcium hydroxide and calcium carbonate are calculated based on the thermal analysis results for carbon dioxide concentration, see Table 5 of the paper. Using data in Pan et al. (2018), we also look at the relationship between carbonation depth and the content of calcium hydroxide and calcium carbonate at different carbon dioxide concentrations, i.e. the natural concentration in the air corresponding to 0.03% for one year, and the accelerated conditions: at concentration of 3% for 28 days and at concentration of 20% for carbonation times of 14 and 28 days. Regardless of the carbon dioxide concentration, the content of calcium hydroxide always increases with depth, and calcium carbonate shows an opposite trend.

Under the condition of high carbon dioxide concentration (20%) after 14 days the Ca(OH)$_2$ content in the completely carbonated zone (0–3 mm) layer was higher than that at a lower carbon dioxide concentration. On the contrary, when the carbonation time is prolonged to 28 days, the residual Ca(OH)$_2$ in the (0–3 mm layer) was almost equal to that in the natural conditions after one year. For this reason, we decided to simulate with our model the case of 20% of carbon dioxide concentration.

In Fig. 4 plots of the profiles derived from experimental data (line-circles) taken from Pan et al. (2018) for carbon dioxide concentration of 20% and the related numerical results obtained by the model (line-points) using parameters in Table 2 at
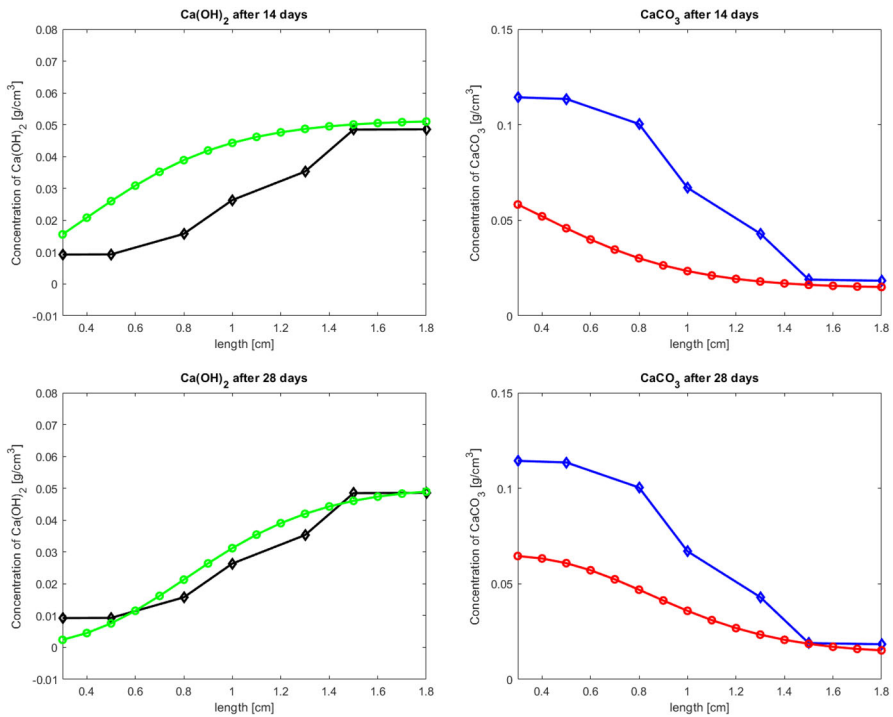
Fig. 4 Plots of the profiles derived from experimental data (line-circles) taken from Pan et al. (2018) and numerical results obtained by the model (line-points) at time $t = 14$ days (top) and at time $t = 28$ days (bottom). On the left: profile of measured versus computed $Ca(OH)_2$ and on the right: profile of measured versus computed $CaCO_3$. The y-axis depicts the concentration of the substances (in g/cm^3), while the x-axis shows the length of the specimen (in cm)

time $t = 14$ days (top) and at time $t = 28$ days (bottom) are depicted. As can be observed from the bottom pictures in Fig. 4 the qualitative behavior for the calcium hydroxide profile is very close to the experimental one after 28 days and it also shows a quantitative accordance from the spatial point of 0.5 cm until the top endpoint of the specimen (1.8–2 cm). For the calcium carbonate depicted in the top pictures of Fig. 4 the situation is a bit different, since there is a qualitative difference between the experimental data VS the numerically obtained profile; moreover, the concentration level is lower for the calcium carbonate computed by the model. Such a different behavior is due to the fact that in the article from which the data was taken only the formation process is detected, while in the model there are two reactions for $CaCO_3$: the formation of calcium carbonate and its dissociation over time. The model, indeed, refers to an ideal concrete, with an initial concentration of $CaCO_3$ equal to zero, and all the calcium carbonate is due only to the carbonation reaction. It is worth noting that experimentally it is difficult to have a sample under these conditions, as the formation of $CaCO_3$ already occurs during the production of the concrete itself.
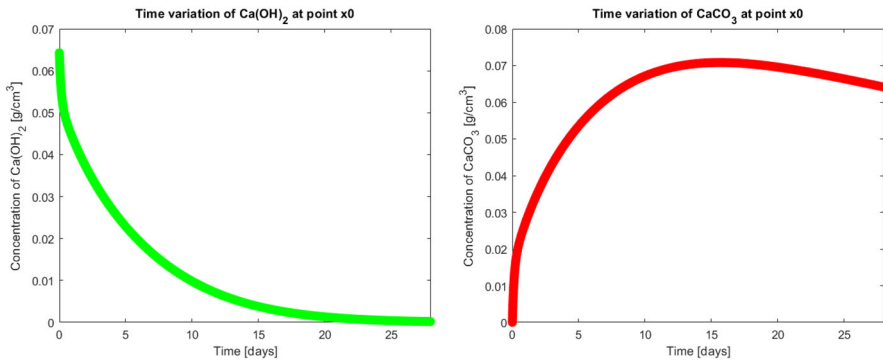
Fig. 5 Plots of the time evolution (in days) of calcium hydroxide (left picture) and calcium carbonate (right picture) concentrations (in units g/cm^3) at $x = x_0$. Parameters assumed as in Table 2

Figure 5 shows the graphs for calcium hydroxide (green line) and calcium carbonate (red line) as a function of time at the starting point x_0, obtained by the model in the time window [0, 28] days for the parameters assumed as in Table 2.

As already seen in the previous graphs, there is a perfect correspondence between the rapid consumption of $Ca(OH)_2$ and the rapid formation of $CaCO_3$, in fact the minimum and maximum of the two curves occur for the same value of time. It should be remembered that the experiment is carried out in conditions of accelerated carbonation (concentration considerably higher than CO_2 in the atmosphere) and that the reactions considered do not take into account the other balances and competitive reactions that can be established inside the concrete, a porous material and therefore continuously exposed to the external environment. In the interpretation of these results it should be taken into account that the real process will not proceed so quickly towards complete carbonation and the simplified hypotheses made will not lead to such clear-cut results, but it is important because in addition to perfectly describing the main phases of the carbonation phenomenon, highlights the possibility that the calcium carbonate dissolution reaction may take place, a reaction responsible for an increase in porosity not foreseen by the other models.

All the simulations were performed with a code developed in Matlab ©. The computational time for a simulation on the complete model with fixed parameters until time $t = 28$ days, takes about 150 s on an Intel(R) Core(TM) i7-3630 QM CPU 2.4 GHz.

6 Conclusion

A mathematical model for the description of the effects of carbonation on concrete has been here developed. Considering the dissolution of calcium carbonate as part of the set of reactions has made it possible to arrive at a more realistic model than those provided in the scientific literature to date. We believe that our results can contribute to the resolution of a long-standing controversy concerning the effects of carbonation on the cement microstructures. The outcomes of our simulations indicate that for long

observation times, porosity tends to increase. This deduction opens up a completely different scenario, as increased porosity implies a major fragility for the cementitious material. A more porous medium has a greater susceptibility to chemical degradation and may also suffer from structural weaknesses. In view of the relevance of the results, the research team intends to continue to develop the topic in a comprehensive manner by setting up ad-hoc laboratory experiments by varying the type of concrete and the atmospherical conditions.

In this respect, a very compelling challenge would be to extrapolate the accelerated testing conditions to real performance as to use accelerated testing for the kinetic study in terms of predicting the degradation rate under natural conditions. The model we are here proposing could be used as a starting point to develop mathematical simulations capable of estimating the change in porosity on cementitious materials exposed for a long time to interaction with atmospheric CO_2. This study will include not only the oldest reinforced concrete structures of civil engineering (roads, bridges, infrastructures) but also buildings of the 20th century that nowadays enter fully into the cultural heritage as buildings of industrial archaeology or works of great architects of the last century such as Le Corbusier. Our interest is to understand how today's increasingly CO_2-rich environment affects the chemical and physical characteristics of old reinforced concrete materials. Such a predictive study of cultural heritage materials is being designed and evolved.

References

Alì, G., Furuholt, V., Natalini, R., Torcicollo, I.: A mathematical model of sulphite chemical aggression of limestones with high permeability: part I modeling and qualitative analysis. Transp. Porous Med. **69**(1), 109–122 (2007)

Anstice, D.J., Page, C.L., Page, M.M.: The pore solution phase of carbonated cement pastes. Cem. Concr. Res. **35**(2), 377–83 (2005)

Ahsraf, W.: Carbonation of cement-based materials: challenges and opportunities. Constr. Build. Mater. **120**(1), 558–570 (2016)

Auroy, M., Poyet, S., Le Bescop, P., Torrenti, J.M., Charpentier, T., Moskura, M., Bourbon, X.: Comparison between natural and accelerated carbonation (3% CO2): impact on mineralogy, microstructure, water retention and cracking. Cem. Concr. Res. **1**(109), 64–80 (2018)

Ball, P.: Water: an enduring mystery. Nature **452**, 291–292 (2008). https://doi.org/10.1038/452291a

Bretti, G., Ceseri, M., Natalini, R.: A moving boundary problem for reaction and diffusion processes in concrete: carbonation advancement and carbonation shrinkage. Discrete Continuous Dynam. Syst. Ser. **15**(8), 2033–2052 (2022). https://doi.org/10.3934/dcdss.2022092

Chang, C.F., Chen, J.W.: The experimental investigation of concrete carbonation depth. Cem. Concr. Res. **36**(9), 1760–7 (2006)

Chapwanya, M., Stockie, J.M., Liu, W.: A model for reactive porous transport during re-wetting of hardened concrete. J. Eng. Math. **65**(1), 53–73 (2009)

Chen, T., Gao, X., Qin, L.: Mathematical modeling of accelerated carbonation curing of Portland cement paste at early age. Cem. Concr. Res. **120**, 187–97 (2019)

Coppola, L.: Concretum. McGraw-Hill, New York (2007)

Coto, B., Martos, C., Peña, J.L., Rodríguez, R., Pastor, G.: Effects in the solubility of CaCO3: experimental study and model description. Fluid Phase Equilibria **25**(324), 1–7 (2012)

Freddi, F., Mingazzi, L.: Phase-field simulations of cover cracking in corroded RC beams. Procedia Struct. Integr. **33**, 371–384 (2021)

Galan, I., Andrade, C., Castellote, M.: Natural and accelerated CO2 binding kinetics in cement paste at different relative humidities. Cem. Concr. Res. **1**(49), 21–8 (2013)

García-González, C.A., Hidalgo, A., Andrade, C., Alonso, M.C., Fraile, J., López-Periago, A.M., Domingo, C.: Modification of composition and microstructure of Portland cement pastes as a result of natural and supercritical carbonation procedures. Ind. Eng. Chem. Res. **45**(14), 4985–4992 (2006)

Groves, G.W., Rodway, D.I., Richardson, I.G.: The carbonation of hardened cement pastes. Adv. Cem. Res. **3**(11), 117–25 (1990)

Hussain, S., Bhunia, D., Singh, S.B.: An experimental investigation of accelerated carbonation on properties of concrete. Eng. J. **20**(2), 29–38 (2016)

Ishida, T., Li, C.H.: Modeling of carbonation based on thermo-hygro physics with strong coupling of mass transport and equilibrium in micro-pore structure of concrete. J. Adv. Concr. Technol. **6**(2), 303–16 (2008)

Kashef-Haghighi, S., Shao, Y., Ghoshal, S.: Mathematical modeling of CO2 uptake by concrete during accelerated carbonation curing. Cem. Concr. Res. **1**(67), 1 (2015)

Leemann, A., Moro, F.: Carbonation of concrete: the role of CO 2 concentration, relative humidity and CO 2 buffer capacity. Mater. Struct. **50**(1), 1–4 (2017)

Mara, A.: Studio della precipitazione del carbonato di calcio. Master degree, Politecnico di Torino (2019)

Meyer, C.: Concrete as a green building material. In: Construction Materials Mindess Symposium (2005 Aug)

Mitchell, M.J., Jensen, O.E., Cliffe, K.A., Maroto-Valer, M.M.: A model of carbon dioxide dissolution and mineral carbonation kinetics. Proc. R. Soc. A Math. Phys. Eng. Sci. **466**(2117), 1265–90 (2010)

Ogino, T., Suzuki, T., Sawada, K.: The formation and transformation mechanism of calcium carbonate in water. Geochim et Cosmochimica Acta **51**(10), 2757–2767 (1987)

Pan, G., Shen, Q., Li, J.: Microstructure of cement paste at different carbon dioxide concentrations. Mag. Concr. Res. **70**(3), 154–62 (2018)

Papadakis, V.G., Vayenas, C.G., Fardis, M.N.: A reaction engineering approach to the problem of concrete carbonation. AIChE J. **35**(10), 1639–50 (1989)

Pedeferri, P.: Corrosione e protezione dei materiali metallici. Polipress (2010)

Peter, M.A., Muntean, A., Meier, S.A., Böhm, M.: Competition of several carbonation reactions in concrete: a parametric study. Cem. Concr. Res. **38**(12), 1385–93 (2008)

Plusquellec, G., Geiker, M.R., Lindgard, J., Duchesne, J., Fournier, B., De Weerdt, K.: Determination of the pH and the free alkali metal content in the pore solution of concrete: review and experimental comparison. Cement Concr. Res. **96**, 13–26 (2017)

Pu, Q., Jiang, L., Xu, J., Chu, H., Xu, Y., Zhang, Y.: Evolution of pH and chemical composition of pore solution in carbonated concrete. Constr. Build. Mater. **28**(1), 519–24 (2012)

Radu, F.A., Muntean, A., Pop, I.S., Suciu, N., Kolditz, O.: A mixed finite element discretization scheme for a concrete carbonation model with concentration-dependent porosity. J. Comput. Appl. Math. **1**(246), 74–85 (2013)

Reale, R., Campanella, L., Sammartino, M.P., Visco, G., Bretti, G., Ceseri, M., Natalini, R., Notarnicola, F.: A mathematical, experimental study on iron rings formation in porous stones. J. Cult. Herit. **1**(38), 158–66 (2019)

Shriver D. F., Atkins P. W., Cooper H. L.: Inorganic Chemistry. W. H. Freeman: New York. NY. (1990)

Sun, J.: Carbonation kinetics of cementitious materials used in the geological disposal of radioactive waste (Doctoral dissertation, UCL (University College London)), (2011)

Talukdar, S., Banthia, N., Grace, J.R.: Carbonation in concrete infrastructure in the context of global climate change-Part 1: experimental results and model development. Cement Concr. Compos. **34**(8), 924–930 (2012)

Thiery, M., Villain, G., Dangla, P., Platret, G.: Investigation of the carbonation front shape on cementitious materials: effects of the chemical kinetics. Cem. Concr. Res. **37**(7), 1047–58 (2007)

Torgal, F Pacheco, Miraldo, S., Labrincha, J.A., De Brito, J.: An overview on concrete carbonation in the context of eco-efficient construction: Evaluation, use of SCMs and/or RAC. Constr. Build. Mater. **36**, 141–150 (2012)

Villain, G., Thiery, M.: Gammadensimetry: a method to determine drying and carbonation profiles in concrete. Ndt & E Int. **39**(4), 328–37 (2006)

Villain, G., Thiery, M., Platret, G.: Measurement methods of carbonation profiles in concrete: thermo-gravimetry, chemical analysis and gammadensimetry. Cem. Concr. Res. **37**(8), 1182–92 (2007)

Zeebe, R.E.: On the molecular diffusion coefficients of dissolved CO2, HCO3-, and CO32-and their dependence on isotopic mass. Geochim. Cosmochim. Acta **75**(9), 2483–98 (2011)

Publisher's Note Springer Nature remains neutral with regard to jurisdictional claims in published maps and institutional affiliations.